RSC Advances

ROYAL SOCIETY OF CHEMISTRY

www.rsc.org/advances

Insight into ETS-10 synthesis for the preparation of mixed matrix membranes for CO_2/CH_4 gas separation

Sara Sorribas,[a] Bibiana Comesaña-Gándara[b], Angel E Lozano[b,c], Beatriz Zornoza,[a] Carlos Téllez[a], and Joaquín Coronas[a,*]

[a]Chemical and Environmental Engineering Department and Instituto de Nanociencia de Aragón (INA), Universidad de Zaragoza, 50018 Zaragoza, Spain.

[b]Department of Macromolecular Chemistry, Institute of Polymer Science and Technology, ICTP-CSIC, 28006 Madrid, Spain

[c]SMAP, UVA-CSIC Research Unit, University of Valladolid, 47011 Valladolid, Spain

*Corresponding author. Phone: (+34) 976762471; Fax: (+34) 976 761879; E-mail: coronas@unizar.es

ABSTRACT

An in-depth study into the synthesis of the titanosilicate ETS-10 has been carried out to obtain crystals with different particle size, roughness and porosity. The effect of these parameters on CO_2/CH_4 gas separation performance using mixed matrix membranes (MMMs) has been studied. MMMs based on ETS-10 polycrystalline particles of 1-2 μm in size with high surface roughness and porosity gave rise to a good filler dispersion and filler-polymer interaction. The addition of 10 wt% ETS-10 polycrystalline particles into polysulfone matrix increased the CO_2 permeability from 6.1 to 7.8 Barrer and the CO_2/CH_4 selectivity from 31 to 38. When using the polyimide 6FDA-6FpDA, a glassy polymer with high gas permeability, the addition of 10 wt% ETS-10 polycrystalline particles increased the CO_2 permeability from 96 to 125 Barrer, with a decrease in CO_2/CH_4 selectivity from 56 to 51.

KEYWORDS: Titanosilicate ETS-10, mixed matrix membranes, polysulfone, polyimide 6FDA-6FpDA, gas separation.

1. INTRODUCTION

ETS-10 is a microporous titanosilicate with the formula $M_2TiSi_5O_{13}.nH_2O$ (where M=K, Na), built from orthogonal TiO_6 octahedra and SiO_4 tetrahedra linked by corner-sharing oxygen atoms forming a three-dimensional pore system with good accessibility for guest molecules.[1] Each Ti atom in a six-coordinated state carries two negative charges balanced by Na^+ and K^+ cations, which give this material a high cation exchange capacity.[2] The synthesis of the titanosilicate ETS-10 was first reported by Kuznicki, who used $TiCl_3$ as the Ti source along with seeds of ETS-4.[3] Since then, substantial efforts have been made to grow highly crystalline pure ETS-10 in conventional hydrothermal syntheses (at temperatures between 150-230 ºC) and short time periods (<48 h).[4] In addition, several studies have focused on controlling nucleation/crystal growth processes as a way to modify the ETS-10 particle size, a critical parameter when synthesizing zeolitic materials for a specific application.[5] For example, while large sizes allow structure refinement from single crystal data and studying the formation of intergrowth structures inside single zeolite crystals,[6, 7] small sizes[8-10] may have applications in the preparation of mixed matrix membranes (MMMs) for molecular separations.

MMMs are an excellent strategy to overcome the trade-off between permeability and selectivity for polymeric membranes. The use of two materials with different gas separation behaviors offers the possibility of designing an efficient membrane combining the advantages of both phases: the easy processability and low cost of the polymer with the superior gas separation performance of the nanostructured fillers.[11-13] Also, the incorporation of these specific materials within the polymeric matrix generally provides

enhanced physical, mechanical and thermal properties for their use in aggressive environments and a membrane stabilization system against changes in permeability with the temperature.[14]

ETS-10 inorganic membranes on α-alumina supports have previously been used in the separation of propylene/propane mixtures,[15, 16] and in the separation of CO_2 mixtures (CO_2/N_2, CO_2/H_2),[17] since ETS-10 is a basic nature material which can adsorb CO_2 at low temperatures.[18] Regarding MMMs based on the titanosilicate ETS-10, Burmann et al.[19] prepared 8 wt% ETS-10-Polysulfone MMMs via spin coating for H_2/CH_4 and O_2/N_2 gas separation mixtures, obtaining a slight improvement in gas permeability/selectivity compared to the bare polymer film. Chitosan (CS) and microporous titanosilicate ETS-10/CS MMMs were prepared and tested for pervaporation of water/ethanol mixture increasing flux with respect to the pure CS membranes.[20]

Polysulfone (PSF), whose structure is shown in Figure 1a, is an important commercial membrane material for gas separation due to its excellent mechanical properties, wide operating temperature range, fairly good chemical resistance, easy fabrication and low price.[21] However, its great rigidity due to its high degree of molecular immobility leads to low permeabilities. To improve the permeability and selectivity of gas separation polymeric membranes, the incorporation of bulky groups in the chains of glassy polymers makes their structure stiffer and hinders an efficient packing of the chains, leading to an increase in free volume. These high volume fractions with restrictive or selective channels increase the diffusivity of gases, and thus their permeability. An example of such a kind of polymer is the fluorinated polyimide 6FDA–6FpDA, whose structure is shown in Figure 1b. Fluorinated polyimides are particularly interesting for gas separation because they have good mechanical, thermal and transport properties.[22] 6FDA-6FpDA is an

aromatic polyimide having two hexafluoropropane moieties. This polyimide is soluble in many common organic solvents including acetone, tetrahydrofuran or chloroform, it has very good thermal stability and shows very good gas separation properties, in particular for mixtures where one of the components is CO_2.[22-25]

Here, the preparation of ETS-10 MMMs based on PSF via casting/solvent evaporation technique (in contrast with our previously reported ETS-10/PSF MMMs prepared by spin coating) is studied. In addition, a more permeable fluorinated polymer, the polyimide 6FDA-6FpDA, is used as polymer matrix for the preparation of ETS-10 MMMs. In order to analyze the effect of the crystal size and morphology of the filler on the membrane performance, several ETS-10 crystals with different size and textural properties are synthesized and the MMMs are evaluated for separation of CO_2/CH_4 mixture. This mixture can be related to bio-methane upgrading, an application of special interest given the renewable character of such source of energy, whose use would contribute to reduce CO_2 emissions.

2. EXPERIMENTAL

2.1. Synthesis of ETS-10 crystals

Several syntheses were carried out by varying different parameters (Ti source, temperature and synthesis time). Table S1 summarizes all the syntheses conditions implemented. The nomenclature used here is "Ti source_ temperature_time". The different procedures followed to synthesize ETS-10 crystals are described below.

2.1.1. Synthesis of ETS-10 crystals using TiO_2

The preparation of ETS-10 crystals using TiO_2-anatase of two different sizes as the Ti source (Ti1 of 200-300 nm and Ti2 of 25 nm, both from Sigma-Aldrich, 99.8 and 99.7 wt%, respectively) was carried out as follows.[5] Firstly, 12.3 g of sodium silicate solution (27 wt% SiO_2, 8 wt% Na_2O, Merck) and 16.5 g of distilled water were mixed. Next, 0.86 g of potassium chloride (99.995 wt%, Panreac), 1.1g of potassium fluoride (99 wt%, Aldrich) and 3.5 g of sodium chloride (pro-analyse, Merck) were added to the mixture under strong stirring. Finally, 0.8 g of TiO_2-anatase was added and stirred for another 30 min to obtain the gel. The pH was measured in a 1/100 diluted portion of the gel, making sure that it was always in the 10.4–10.6 range to avoid impurities.[26] The resulting gel was poured into a Teflon-lined autoclave and submitted to hydrothermal synthesis at the desired temperature and time. After that, the autoclave was removed from the oven and quenched under cold tap water to room temperature. The product was centrifuged several times with water and dried at 100 ºC overnight.

2.1.2. Synthesis of ETS-10 crystals using $TiCl_3$

For the preparation of ETS-10 crystals with $TiCl_3$ as the Ti source, the following hydrothermal synthesis procedure was used.[5] Firstly, 5.1 g of $TiCl_3$ (15 wt% $TiCl_3$ in 10 wt% HCl, Merck) was mixed with 21.4 g of distilled water. To convert $TiCl_3$ to $TiCl_4$, 0.66 g of hydrogen peroxide (30 wt%, Sigma-Aldrich) was added. After that, 0.86 g of potassium chloride (99.995 wt%, Panreac), 1.0 g of sodium hydroxide (extra pure, Scharlau) and 6.1 g of sodium silicate solution were added under strong stirring. For seeding, previously prepared 500 nm ETS-10 crystals (synthesis Ti2_180_48h) in 0.3 wt% with respect to the total weight of the gel were added at the end. After complete mixing of the precursors for 30 min, the procedure was the same as for syntheses with TiO_2. It is

worth mentioning that for the syntheses with $TiCl_3$ carried out at 180 ºC or at two stages (180-230 ºC), the molar gel composition used was diluted twice.

2.2. Synthesis of polyimide 6FDA-6FpDA

The synthesis of high molecular weight 6FDA-6FpDA was carried out by reacting the dianhydride 6FDA and the aromatic diamine, 6FpDA, through an *in situ* silylation base-assisted process.[27, 28] Both monomers were purified by sublimation under high vacuum (220 ^{o}C for 6FDA and 190 ^{o}C for 6FpDA, respectively).

A three-neck flask was equipped with a mechanical stirrer and a nitrogen inlet and outlet. The flask was filled with 20 mmol of 6FpDA diamine and 20 mL of N,N-dimehtylacetamide (DMAc), which was employed as the solvent. The mixture was stirred at room temperature until all the solid had dissolved. Then, the solution was cooled to 0 ^{o}C and the required amount of trimethylchlorosilane (TMSCl) (1mol/mol amino group, 40 mmol) was slowly added, followed by the addition of pyridine (1mol base/mol amino group, 40 mmol). The solution was heated to room temperature and stirred for 15 min to ensure the formation of the silylated diamine in the appropriate cases. After this time, the solution was once more cooled to 0°C, and 20 mmol of 6FDA was rapidly added along with 15 mL of DMAc. Finally, a small amount of 4-dimethylamine pyridine (DMAP) (0.1 mol/mol amino group, 4 mmol) was added followed by 5.0 mL of solvent. The reaction mixture was then stirred for 15 min at 0 °C after which the temperature was raised to room temperature and left overnight.

Cyclodehydration of the formed polyamic acid was accomplished by using an acetic anhydride (60 mmol)/Py (60 mmol) mixture. The reaction mixture was stirred at room

temperature for 6h followed by heating for a further hour at 60 °C. Afterwards, the flasks were cooled down to room temperature and the resulting polymer solutions were precipitated into 1000 mL of water, washed several times with water and extracted in a sohxlet extractor with ethanol to remove traces of solvent and oligomers. The 6FDA-6FpDA polymer was dried overnight under vacuum at 200 ^{o}C in order to remove the occluded solvent. Yields over 91% were obtained.

2.3. Preparation of MMMs

Two different polymers were used as matrices to prepare MMMs, commercial PSF (Aldrich, Mw 35000) and polyimide 6FDA-6FpDA. ETS-10 MMMs were prepared by the casting/solvent evaporation technique using chloroform as solvent. Firstly, 3.6 g and 4.2 g of chloroform (Sigma Aldrich, 99%) for PSF and 6FDA-6FpDA based MMMs, respectively, together with the amount of ETS-10 necessary to obtain the required loading (10-20 wt%) were mixed, keeping the amount of ETS-10 + polymer = 0.4 g. The polymer (PSF or 6FDA-6FpDA) was then added and the resulting dispersion was stirred overnight. The suspension was then sonicated with three intervals of 15 min, cast on a flat glass plate and then left overnight, partially covered to slow down the natural evaporation of solvent under ambient conditions. Once dried at room temperature, the films were placed for 24 h under 1 kPa pressure in a vacuum oven at 120 ^{o}C for PSF based MMMs and at 180 ºC for 6FDA-6FpDA based MMMs to remove the remaining solvent.

2.4. Characterization

To analyze the ETS-10 particle size and morphology, and to evaluate their dispersion and the contact between the ETS-10 and the polymeric phase, both ETS-10

powder and the MMMs were characterized by scanning electron microscopy (SEM) using an Inspect F scanning electron microscope. Prior to observation, the samples were coated with 15 nm of platinum. MMM cross sections were prepared by freeze-fracturing after immersion in liquid N_2 before coating.

The ETS-10 samples and MMMs based on 6FDA-6FpDA were also characterized by X-ray diffraction (XRD) at room temperature using a D-Max Rigaku diffractometer with a copper anode and a graphite monochromator to select Cu-$K_{\alpha 1}$ radiation (λ= 1.5418 Å).

Nitrogen adsorption-desorption isotherms were measured at 77 K using a porosity analyzer (TriStar 3000, Micromeritics Instrument Corp.). The samples were outgassed with a heating rate of 10 ºC/min until 200 ºC and maintained for 8 h. BET specific surface areas were measured from the adsorption branches in the relative pressure range of 0.05-0.25 and external surface areas were calculated using the t-plot method.

2.5. Permeation measurements

The gas permeation equipment used in the study is described elsewhere.[29] For permeation tests, 13.8 cm^2 circular membranes were cut from the films prepared as described above. The membrane samples were placed in a module consisting of two stainless steel pieces and a macroporous disk support 316LSS of 20 µm nominal pore size, gripped inside with Viton o-rings. An equimolar mixture of 25/25 cm^3(STP)/min CO_2/CH_4 stream was fed at 330 kPa to the retentate side of the membrane using mass-flow controllers, while the permeate side of the membrane was swept with a 2 cm^3(STP)/min mass-flow controlled stream of helium at 125 kPa. The differential pressure between the retentate and the permeate side (ΔP) was 205 kPa. Concentrations of CO_2 and CH_4 in the outgoing streams were analyzed by an Agilent 3000A online gas microchromatograph

equipped with a thermal conductivity detector. Permeability in Barrer ($1 \cdot 10^{-10}$ $cm^3(STP) \cdot cm/(cm^2 \cdot s \cdot cmHg)$) was calculated once the exit stream of the membrane was stabilized, and the separation selectivity was calculated as the ratio of permeabilities. To calculate the ideal selectivity and compare the results with those given in the literature, single gas measurements were also carried out for 6FDA-6FpDA membranes by feeding 50 $cm^3(STP)/min$ of individual gases, CO_2 and CH_4, at 330 kPa. The temperature of the experiments was controlled at 35 ºC.

3. RESULTS AND DISCUSSION

3.1. Characterization of ETS-10 crystals

To obtain ETS-10 crystals with different particle size and roughness, several syntheses were carried out by varying parameters such as the Ti source, temperature and synthesis time (see Table S1 in the Supporting Information). In brief, from a reference synthesis at 230 ºC using $TiCl_3$,[5, 30] the temperature was decreased down to 180 ºC and/or TiO_2 anatase of two different sizes (25 and 200-300 nm) was used as a low solubility Ti source to slow the crystal growth and thus have an effect on the particle size. The aim of testing different ETS-10 crystals as fillers was to study the effect of the particle size on the separation performance of the MMMs and to improve the bonding established between the polymer and the filler by increasing the external roughness of the ETS-10 particles.[31]

Figures 2 and 3 and Table 1 show SEM images, X-ray diffraction patterns and textural properties, respectively, of the different samples selected for the preparation of the MMMs. Table 1 also shows the ETS-10 particle size, in both c and a=b directions.[32]

Sample Ti2_180_48h (Figure 2.a) was synthesized with TiO_2-anatase nanoparticles (25 nm), which led to a heterogeneous primary nucleation of ETS-10.[5] This, together with its low solubility, dramatically reduced the availability of nutrients for growth, leading to small ETS-10 particles (0.44 x 0.21 μm). It is worth mentioning that at 180 ºC it was not possible to obtain ETS-10 crystals with Ti1 (200-300 nm), since this Ti source needs higher temperatures to be dissolved. In general, when using the same synthesis conditions (i.e. 230 ºC and 48 h), larger crystal particles were obtained with $TiCl_3$ (see Table S1 and Figure S1, Supporting information), due to the promotion of crystal growth over nucleation when this more soluble Ti source was used.[5]

When the temperature was reduced to 180 ºC and the molar gel was diluted (sample $TiCl_3$_180_48h), nanocrystals of 80 ±20 nm were obtained (Figure 2.b) with the presence of amorphous gel detected by XRD (see Figure 3). This fact could be due to the low temperature used, which was insufficient to dissolve all the nutrients for crystal growth. It is worth mentioning that this is the smallest particle size ever reported for this material.[5, 26, 30, 33] In sample Ti2_180_48h, ETS-4 and TiO_2-anatase impurities were also present (see Figure 3).

To increase the crystallinity of the $TiCl_3$_180_48h sample, after 48 h at 180 ºC the gel synthesis was heated up to 230 ºC and maintained for 2 h (sample $TiCl_3$_180-230_48-2h, Figure 2c) and 24 h (sample $TiCl_3$_180-230_48-24h, Figure 2d). The increase in synthesis temperature to 230 ºC increased the particle size to 1.2±0.2 μm and 1.9±0.3 μm after 2 h and 24 h, respectively. The crystallinity and porosity of these two samples were also higher than those for the $TiCl_3$_180_48h sample (see Figure 3 and Table 1), indicating that when $TiCl_3$ is used, temperatures higher than 180 ºC are needed to crystallize the

titanium and silicon nutrients. SEM images of these samples (Figure 2c,d) show particles consisting of polycrystalline aggregates that became twin crystals after 24 h, different from those of the $TiCl_3$_230_24h sample (Figure S1b, Supporting information) which exhibits the typical truncated pyramidal crystal shape. The particles in Figure 2c,d show an evident surface roughness that could be due to two reasons. Firstly, the dilution of the initial synthesis mixture resulting in crystal clusters, as previously reported.[4] Secondly, the presence of ETS-10 nanocrystals (Figure 2b) generated at the 180 ºC stage that act as seeds when the temperature is increased to 230 ºC and grow close each other, creating polycrystalline particles.

The external surface of these samples was in accordance with their particle size and roughness. The $TiCl_3$_180_48h sample had the highest external surface area (59 m^2g^{-1}) due to its having the smallest particle size (80 nm) in addition to the particle agglomeration that led to capillarity condensation between the crystals. Furthermore, samples $TiCl_3$_180-230_48-2h and $TiCl_3$_180-230_48-24h have extra roughness due to the intercrystalline regions, leading to high external specific surface areas (41-42 m^2g^{-1}). To increase this external area value, other strategies such as postsynthesis treatment with hydrogen peroxide under microwave irradiation has been reported,[34] creating mesopores within the ETS-10 structure that increased the external surface area of this material up to 70 m^2g^{-1}.

3.2. Characterization of the membranes

3.2.1. ETS-10 MMMs based on polysulfone (PSF)

Figure 4 shows SEM images of the different ETS-10 MMMs based on PSF. The filler is distributed homogeneously within the polymer and an intimate filler-polymer

interaction is suggested, especially for samples $TiCl_3$_180-230_48-2h and $TiCl_3$_180-230_48-24h (Figure 4.c, d) where, due to the roughness of the polycrystalline particles, polymer chains enter into the intercrystalline spaces, giving rise to an interpenetrated filler–polymer composite.[31] Some particle agglomeration can be observed for samples Ti2_180_48h and $TiCl_3$_180_48h (Figure 4.a,b) due to the small particle size of these fillers.

Table 2 and Figure 5 shows the gas separation results for the CO_2/CH_4 mixture of 10 wt% MMMs based on PSF with different ETS-10 samples. For Ti2_180_48h and $TiCl_3$_180_48h MMMs, the ETS-10 agglomerations observed by SEM created voids between the particles that could explain the decrease in CO_2/CH_4 selectivity. In addition, the slight decrease in CO_2 permeability could be due to the low porosity of $TiCl_3$_180_48h sample and the presence of non-porous anatase as impurity in the Ti2_180_48h sample. MMMs using samples $TiCl_3$_180-230_48-2h and $TiCl_3$_180-230_48-24h as fillers increased both their CO_2 permeability and CO_2/CH_4 selectivity in comparison with pure polymer. This can be explained by the fact that, in addition to the high porosity of these fillers and the good filler-polymer interaction, ETS-10 preferentially adsorbs CO_2 over CH_4,[35] probably because of the significantly greater quadrupole moment and polarizability of CO_2 molecules. Furthermore, adsorbed CO_2 is expected to reduce the CH_4 permeation by hindrance, resulting in overall CO_2 selectivity in CO_2/CH_4 mixtures.[17] Thus, because of two concomitant effects, i. e., the diffusion and sorption paths created in the membrane when ETS-10 crystals are added and the optimized filler-polymer contact, the pursued trend of increasing both the permeability and selectivity with the addition of the filler was achieved.

3.2.2. 6FDA-6FpDA membranes

In order to improve the performance of the MMMs, the more permeable polyimide 6FDA-6FpDA was chosen as the polymeric matrix. Table 3 shows the results obtained for the separation of CO_2/CH_4 mixtures using pure 6FDA-6FpDA membranes. For the separation of CO_2/CH_4 equimolar mixtures, CO_2 permeability of 96 ± 1 Barrer (in comparison with 6.1 ± 0.2 Barrer for pure PSF) with a CO_2/CH_4 selectivity of 56 ± 3 (31 ± 1 for pure PSF) were obtained. These high values can be explained because of the presence of bulky groups ($-CF_3$) that increases the free volume and makes the structure stiffer, leading to more permeable and selective membranes. In addition, the high solubility of the condensable CO_2 gas in the polymer and its lower kinetic diameter (0.33 nm) in comparison with CH_4 (0.38 nm) also contribute to obtaining simultaneously high permeability and selectivity for this mixture, being close to the 2008 Robeson upper bound.[36] It is worth mentioning that the single gas measurements were similar to those reported in the literature based on the "time lag" method, at 35 ºC and 1 bar (see Table 3, errors corresponding to membranes manufactured with different solvents).[22] The fact that ideal selectivity (from single gas measurements) was lower than that obtained with binary mixtures suggests an apparent competitive adsorption of the gases favorable to CO_2. In consequence, in binary mixtures the permeability of CH_4 decreases due to the faster diffusion of the smaller and more strongly adsorbed CO_2 gas molecule.[29] Furthermore, CO_2 permeability was higher for the binary mixture than for single gas. Since the total feed pressure was kept constant, the CO_2 partial pressure gradient was double for single gas measurements than for those with a binary mixture. Thus, as the CO_2 pressure increases, the membrane become saturated and therefore the permeability decreases.[37]

3.2.3. ETS-10 MMMs based on 6FDA-6FpDA

From the results obtained with ETS-10/PSF MMMs, $TiCl_3$_180-230_48-2h was chosen for the preparation of MMMs based on 6FDA-6FpDA. This polycrystalline filler had the smallest particle size (1.2 μm) and the highest BET area and in consequence gave the best membrane performance in the PSF matrix (7.8 Barrer of CO_2 permeability together with CO_2/CH_4 selectivity of 38). Even though SEM images of ETS-10 MMMs at 10 wt% and 20 wt% loading (Figures 6a and b, respectively) suggest an interpenetrated filler–polymer interaction, which could be a result of H-bonding between the external ETS-10 hydroxyl groups[38] and the imide groups of the polyimide, a decrease in selectivity with the addition of the filler indicates the presence of some defects, as will be discussed below. Particle agglomeration at 20 wt% filler loading can be observed, especially at the bottom of the membrane.

The XRD pattern of the MMMs (Figure 7) matches the pattern of the filler, and the signal peaks related to ETS-10 increased with the filler loading, confirming that the particles preserved their structure inside the polymeric matrix.

Compared to bare polymer, ETS-10 MMMs with 10 wt% loading showed an improvement in the CO_2 permeability from 96±1 to 125±1 Barrer, with a slight decrease in CO_2/CH_4 selectivity from 56±3 to 51±2. The fact that CO_2/CH_4 selectivity did not improve with the addition of ETS-10 could be explained from the selectivity value reported for ETS-10 for CO_2/N_2 mixtures (similar to CO_2/CH_4 mixtures) using a continuous ETS-10 membrane.[17] Although defects along the continuous ETS-10 membrane could modify this value, the reported CO_2/N_2 selectivity was 10.8, much lower than that for the 6FDA-6FpDA polymer. In the case of the MMMs, the defects may correspond to the ETS-10-6FDA-6FpDA polymer gaps or non-selective transport pathways through the intercrystalline

spaces of the ETS-10 particles, since the ideal CO_2/CH_4 selectivity for ETS-10 crystals (calculated from adsorption data in the Henry's law region using the Langmuir equation) is 357 at 25 ºC.[35] When higher amounts of this filler were added (20 wt%), the permeability increased to 183 Barrer but the CO_2/CH_4 selectivity dramatically decreased to 13, due to the increase in the formation of non-selective filler-polymer voids caused by particle agglomeration at high loadings. It can be said that the presence of defects in 6FDA-6FpDA based MMMs do not compensate, in terms of separation performance, the enhancement achieved in the filler-polymer interaction by modification of the textural properties of the filler. In any event, the CO_2/CH_4 separation performance of pure polymer and 10 wt% ETS-10 MMM are represented in the 2008 Robeson upper bound (Figure 5), where the results obtained with these membranes are close to the commercially attractive zone.

4. CONCLUSIONS

Adjusting the synthesis conditions (Ti source and synthesis time and temperature) enabled titanosilicate ETS-10 crystalline particles with different sizes and roughness to be obtained. The effect of these parameters on the separation performance was studied using polysulfone as the polymeric matrix. When ETS-10 syntheses were carried out in two steps ($TiCl_3$_180-230_48-2h and $TiCl_3$_180-230_48-24h samples), polycrystalline particles of 1-2 μm in size with high roughness and porosity were obtained, leading to a better filler dispersion and filler-polymer interaction with the polymer matrix. Their use as filler increased the permeoselectivity of pure polysulfone and improved the permeability of polyimide 6FDA-6FpDA membranes, giving results close to the Robeson upper bound. In addition, for polyimide 6FDA-6FpDA membranes the effect of working with individual

gases rather than CO_2/CH_4 mixture on the membrane performance was also studied, suggesting a CO_2 preferential adsorption that enhanced the CO_2/CH_4 separation ability of the MMMs.

Acknowledgments

Financial support from the Spanish Ministry of Economy and Competitiveness (MAT2011-25513, MAT2013-45071-R and MAT2013-40556-R) and DGA Program fellowships (S. S.) from the Regional Government of Aragón and the ESF are gratefully acknowledged. We acknowledge the use of the Servicio General de Apoyo a la Investigación-SAI (Universidad de Zaragoza). All the microscopy work was done in the Laboratorio de Microscopías Avanzadas at the Instituto de Nanociencia de Aragón (LMA-INA). The authors acknowledge the LMA-INA for offering access to their instruments and expertise.

REFERENCES

1. A. Anson, Y. Wang, C. C. H. Lin, T. M. Kuznicki and S. M. Kuznicki, *Chem. Eng. Sci.*, 2008, 63, 4171-4175.

2. J. H. Choi, S. D. Kim, Y. J. Kwon and W. J. Kim, *Microporous Mesoporous Mater.*, 2006, 96, 157-167.

3. S. M. Kuznicki, **1989** US Patent N^{o}. 4853202 (1989).

4. Z. Ji, B. Yilmaz, J. Warzywoda and A. Sacco Jr, *Microporous Mesoporous Mater.*, 2005, 81, 1-10.

5. C. Casado, Z. Amghouz, J. R. García, K. Boulahya, J. M. González-Calbet, C. Téllez and J. Coronas, *Mater. Res. Bull.*, 2009, 44, 1225-1231.

6. X. Wang and A. J. Jacobson, *Chem. Commun.*, 1999, 973-974.

7. M. Navarro, E. Mateo, B. Diosdado, M. Tsapatsis and J. Coronas, *RSC Adv.*, 2015, 5, 18035-18040.

8. L. Tosheva and V. P. Valtchev, *Chem. Mater.*, 2005, 17, 2494-2513.

9. S. B. Tantekin-Ersolmaz, C. Atalay-Oral, M. Tatlıer, A. Erdem-Senatalar, B. Schoeman and J. Sterte, *J. Membr. Sci.*, 2000, 175, 285-288.

10. B. Seoane, J. M. Zamaro, C. Tellez and J. Coronas, *RSC Adv.*, 2011, 1, 917-922.

11. T. S. Chung, L. Y. Jiang, Y. Li and S. Kulprathipanja, *Prog. Polym. Sci.*, 2007, 32, 483-507.

12. M. Rezakazemi, A. Ebadi Amooghin, M. M. Montazer-Rahmati, A. F. Ismail and T. Matsuura, *Prog. Polym. Sci.*

13. M. M. Khan, V. Filiz, G. Bengtson, S. Shishatskiy, M. M. Rahman, J. Lillepaerg and V. Abetz, *J. Membr. Sci.*, 2013, 436, 109-120.

14. A. Brunetti, F. Scura, G. Barbieri and E. Drioli, *J. Membr. Sci.*, 2010, 359, 115-125.

15. I. Tiscornia, S. Irusta, P. Prádanos, C. Téllez, J. Coronas and J. Santamaría, *J. Phys. Chem. C*, 2007, 111, 4702-4709.

16. I. Tiscornia, S. Irusta, C. Téllez, J. Coronas and J. Santamaría, *J. Membr. Sci.*, 2008, 311, 326-335.

17. I. Tiscornia, I. Kumakiri, R. Bredesen, C. Téllez and J. Coronas, *Sep. Purif. Technol.*, 2010, 73, 8-12.

18. F. X. L. i. Xamena and A. Zecchina, *Phys. Chem. Chem. Phys.*, 2002, 4, 1978-1982.

19. P. Burmann, B. Zornoza, C. Téllez and J. Coronas, *Chem. Eng. Sci.*, 2014, 107, 66-75.

20. C. Casado-Coterillo, F. Andrés, C. Téllez, J. Coronas and Á. Irabien, *Sep. Sci. Technol.*, 2014, 49, 1903-1909.

21. D. F. Sanders, Z. P. Smith, R. Guo, L. M. Robeson, J. E. McGrath, D. R. Paul and B. D. Freeman, *Polymer*, 2013, 54, 4729-4761.

22. R. Recio, L. Palacio, P. Prádanos, A. Hernández, Á. E. Lozano, Á. Marcos, J. G. de la Campa and J. de Abajo, *J. Membr. Sci.*, 2007, 293, 22-28.

23. R. Wang, C. Cao and T.-S. Chung, *J. Membr. Sci.*, 2002, 198, 259-271.

24. R. Recio, L. Palacio, P. Prádanos, A. Hernández, Á. E. Lozano, Á. Marcos, J. G. de la Campa and J. de Abajo, *Desalination*, 2006, 200, 225-226.

25. A. Tena, L. Fernández, M. Sánchez, L. Palacio, A. E. Lozano, A. Hernández and P. Prádanos, *Chem. Eng. Sci.*, 2010, 65, 2227-2235.

26. L. Lv, F. Su and X. S. Zhao, *Microporous Mesoporous Mater.*, 2004, 76, 113-122.

27. D. M. Muñoz, J. G. de la Campa, J. de Abajo and A. E. Lozano, *Macromolecules*, 2007, 40, 8225-8232.

28. D. M. Muñoz, M. Calle, J. G. d. l. Campa, J. d. Abajo and A. E. Lozano, *Macromolecules*, 2009, 42, 5892–5894.

29. S. Sorribas, B. Zornoza, C. Tellez and J. Coronas, *J. Membr. Sci.*, 2014, 452, 184-192.

30. J. Rocha, A. Ferreira, Z. Lin and M. W. Anderson, *Microporous Mesoporous Mater.*, 1998, 23, 253-263.

31. B. Zornoza, O. Esekhile, W. J. Koros, C. Tellez and J. Coronas, *Sep. Purif. Technol.*, 2011, 77, 137-145.

32. N. C. Jeong, M. H. Lee and K. B. Yoon, *Angew. Chem. Int. Ed.,* 2007, 46, 5868-5872.

33. N. C. Jeong, Y. J. Lee and K. B. Yoon, *Microporous Mesoporous Mater.*, 2008, 115, 308-313.

34. C. C. Pavel, R. Palkovits, F. Schüth and W. Schmidt, *J. Catal.*, 2008, 254, 84-90.

35. F. Mani, J. A. Sawada and S. M. Kuznicki, *Microporous Mesoporous Mater.*, 2015, 204, 43-49.

36. L. M. Robeson, *J. Membr. Sci.*, 2008, 320, 390-400.

37. C. A. Scholes, G. Q. Chen, G. W. Stevens and S. E. Kentish, *J. Membr. Sci.*, 2010, 346, 208-214.

38. P. D. Southon and R. F. Howe, *Chem. Mater.*, 2002, 14, 4209-4218.

Figure captions

Figure 1. Molecular structure of a) PSF, b) polyimide 6FDA-6FpDA.

Figure 2. SEM images of ETS-10 samples used for MMM preparation: a) Ti2_180_48h, b) $TiCl_3$_180_48h, c) $TiCl_3$_180-230_48-2h, d) $TiCl_3$_180-230_48-24h.

Figure 3. XRD of ETS-10 samples used for MMM preparation: conventional ETS-10 synthesis ($TiCl_3$_230_24h), Ti2_180_48h, $TiCl_3$_180_48h, $TiCl_3$_180-230_48-2h and $TiCl_3$_180-230_48-24h. E and A letters refer to ETS-4 and anatase impurities, respectively.

Figure 4. SEM images of cross-sections of 10 wt% MMMs based on PSF with different ETS-10 samples, a) Ti2_180_48h, b) $TiCl_3$_180_48h, c) $TiCl_3$_180-230_48-2h, d) $TiCl_3$_180-230_48-24h.

Figure 5. Results of pure polymers and 10 wt% MMMs for CO_2/CH_4 mixture at 35 ºC.

Figure 6. SEM images of cross-sections of $TiCl_3$_180-230_48-2h MMMs based on 6FDA-6FpDA with different filler loadings, a) 10wt%, b) 20 wt%.

Figure 7. XRD patterns of $TiCl_3$_230_24h ETS-10, polyimide 6FDA-6FpDA and $TiCl_3$_180-230_48-2h ETS-10 MMMs (10 and 20 wt% loading).

Figure 1

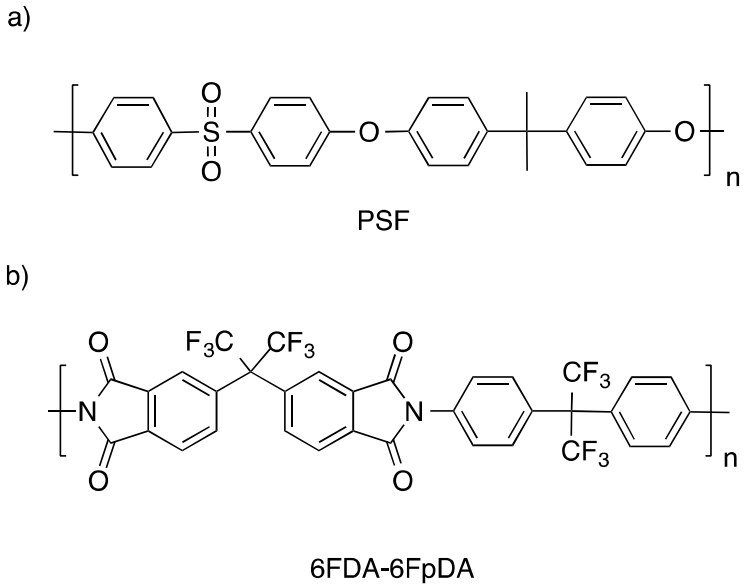

Figure 1. Molecular structure of a) PSF, b) polyimide 6FDA-6FpDA.

Figure 2

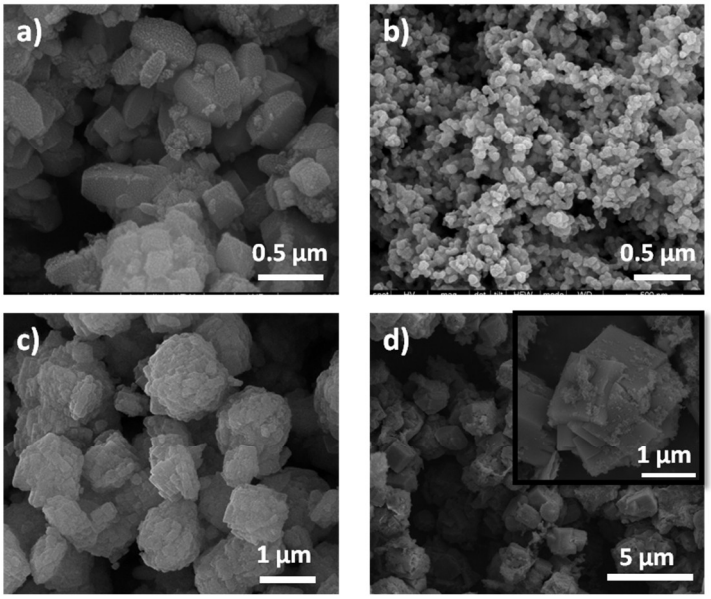

Figure 2. SEM images of ETS-10 samples used for MMM preparation: a) Ti2_180_48h, b) $TiCl_3$_180_48h, c) $TiCl_3$_180-230_48-2h, d) $TiCl_3$_180-230_48-24h.

Figure 3

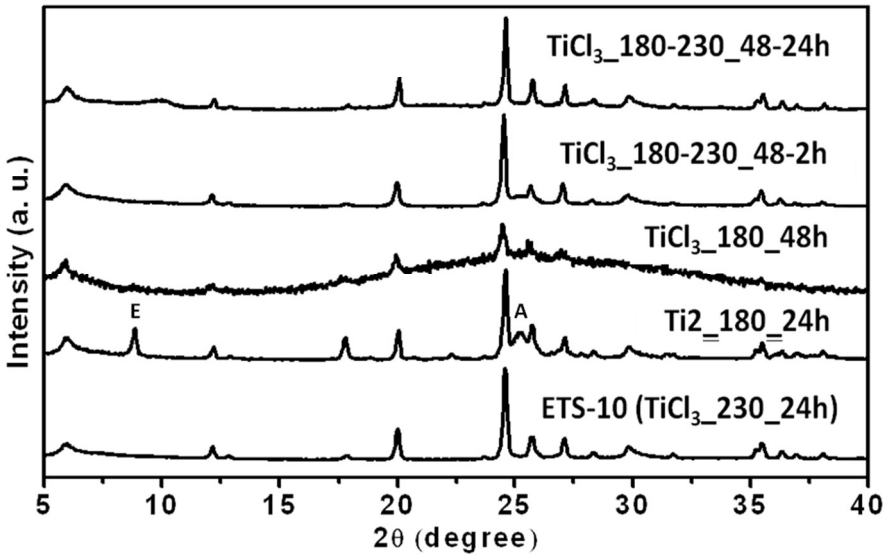

Figure 3. XRD of ETS-10 samples used for MMM preparation: conventional ETS-10 synthesis ($TiCl_3$_230_24h), Ti2_180_48h, $TiCl_3$_180_48h, $TiCl_3$_180-230_48-2h and $TiCl_3$_180-230_48-24h. E and A letters refer to ETS-4 and anatase impurities, respectively.

Figure 4

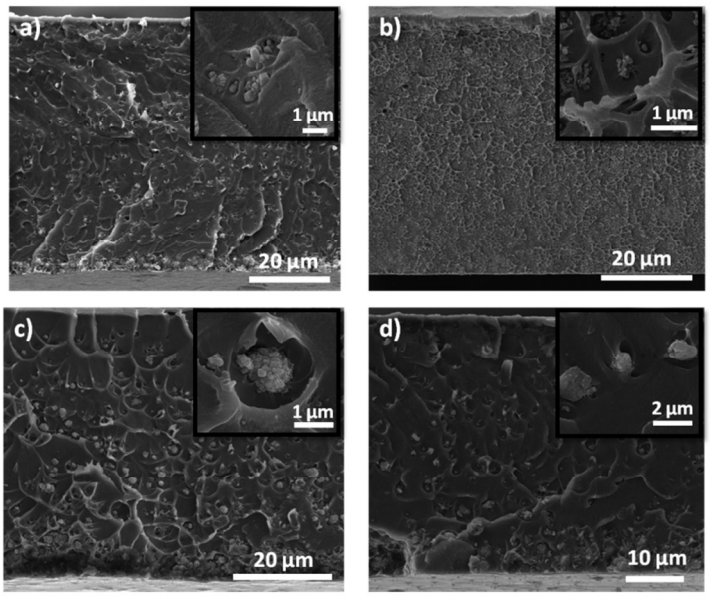

Figure 4. SEM images of cross-sections of 10 wt% MMMs based on PSF with different ETS-10 samples, a) Ti2_180_48h, b) $TiCl_3$_180_48h, c) $TiCl_3$_180-230_48-2h, d) $TiCl_3$_180-230_48-24h.

Figure 5

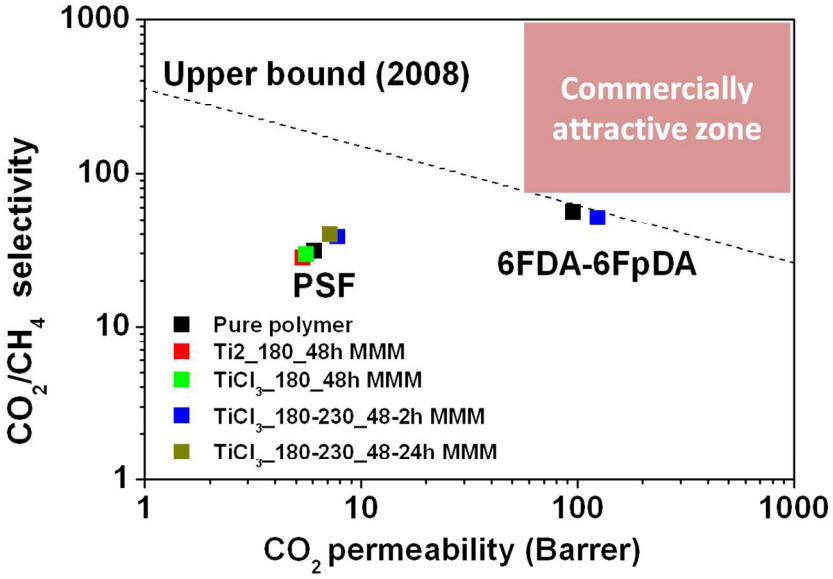

Figure 5. Results of pure polymers and 10 wt% MMMs for CO_2/CH_4 mixture at 35 ºC.

Figure 6

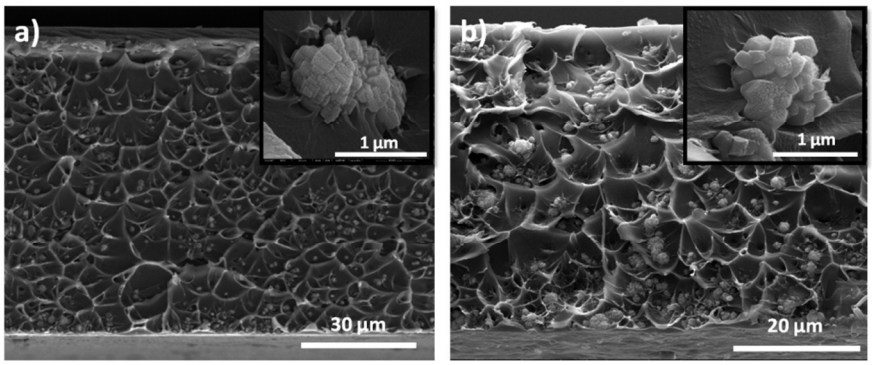

Figure 6. SEM images of cross-sections of $TiCl_3$_180-230_48-2h MMMs based on 6FDA-6FpDA with different filler loadings, a) 10 wt%, b) 20 wt%.

Figure 7

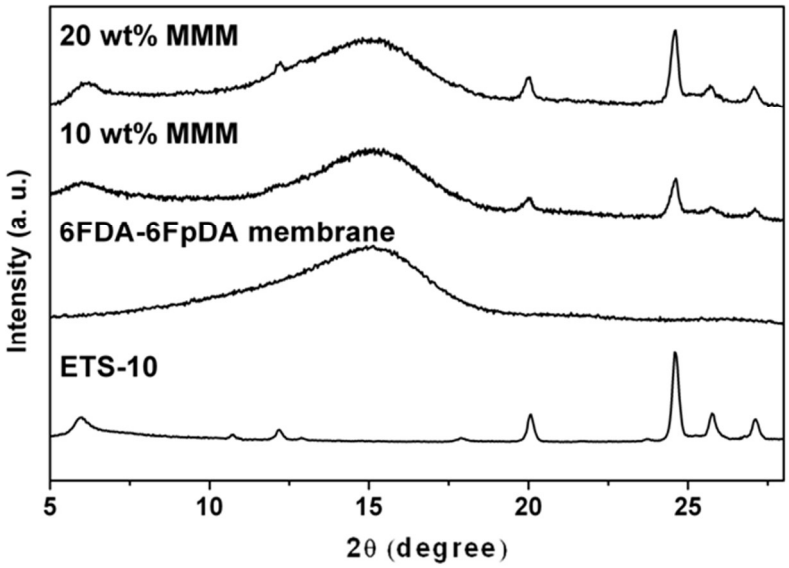

Figure 7. XRD patterns of $TiCl_3$_230_24h ETS-10, polyimide 6FDA-6FpDA and $TiCl_3$_180-230_48-2h ETS-10 MMMs (10 and 20 wt% loading).

Table captions

Table 1. Textural properties of the different samples.

Table 2. Gas separation results for ETS-10 MMMs at 10 wt% loading for equimolar CO_2/CH_4 mixtures at 35 ^{o}C, ΔP=205 kPa. Pure PSF values are the average and standard deviation of three different membranes.

Table 3. CO_2/CH_4 gas separation results for pure 6FDA-6FpDA membranes at 35 $^{\circ}$C.

Table 1

Table 1. Textural properties of the different samples.

ETS-10 sample	S_{BET} (m^2g^{-1})	S_{ext} (m^2g^{-1})	Particle size (µm)
Conventional $TiCl_3$_230_24h	289 ± 4	20	1.9 x 2.3[a]
Ti2_180_ 48h	206 ± 5	30	0.44 x 0.21[a]
$TiCl_3$_180_ 48h	94 ± 0	59	0.08 ± 0.02
$TiCl_3$_180-230_48-2h	318± 5	42	1.2 ± 0.2
$TiCl_3$_180-230_48-24h	166 ± 3	41	1.9 ± 0.3

[a] The first value corresponds to crystal size in direction c, and the second value to crystal size in directions a=b [32].

Table 2

Table 2. Gas separation results for ETS-10 MMMs at 10 wt% loading for equimolar CO_2/CH_4 mixtures at 35 ^oC, ΔP= 205 kPa. Pure PSF values are the average and standard deviation of three different membranes.

Sample	CO_2 permeability (Barrer)	Selectivity CO_2/CH_4
Pure PSF	6.1 ± 0.2	31 ± 1
Ti2_180_48h	5.4	28
$TiCl_3$ 180_48h	5.6	29
$TiCl_3$ 180-230_48-2h	7.8	38
$TiCl_3$ 180-230_48-24h	7.2	40

Table 3

Table 3. CO_2/CH_4 gas separation results for pure 6FDA-6FpDA membranes at 35 °C.

Measurement	CO_2 permeability (Barrer)	CO_2/CH_4 selectivity
Binary mixture (ΔP= 205 kPa)	96±1[a]	56±3[a]
Single gas (ΔP= 205 kPa)	85.1	41.3
Single gas "time lag" method (literature)[22] (ΔP= 101 kPa)	73±6[b]	44±2[b]

[a] The standard deviation was calculated from two different membranes.
[b]The standard deviation was calculated from membranes prepared with different solvents (dichloromethane, tetrahydrofuran, N,N-dimethylacetamide, N,N-dimethylformamide and acetone)